

Numerical study of the natural convection flow resulting from the combined buoyancy effects of thermal and mass diffusion in a cavity with differentially heated side walls

L. Ben Snoussi^{a*}, R. Chouikh^b, A. Guizani^a

^a*INRST, BP 95 Hamam-lif 2050, Tunisia*

Fax 216 71 430 934;

emails: lotfi.snoussi@fst.rnu.tn, amenallah.guizani@inrst.rnrt.tn

^b*IPEIN, Campus Universitaire Merazka 8000,
Nabeul Tunisia*

Received 18 February 2005; accepted 10 March 2005

Abstract

This work is part of general study dealing with the improvement of the distillation rate in solar distillation systems. We are interested in the laminar flow which arises in fluids due to the interaction of the gravity force and density differences caused by the simultaneous diffusion of thermal energy and of chemical species. Species concentration levels are assumed small, as it is typical for many processes in water and in atmospheric air. This study states the problem in a Cartesian coordinates system, involves the use of a Control-Volume based Finite Element Method (CVFEM) and solves the full vorticity transport equation together with the stream function, concentration and energy equations. The predicted stream function patterns, mass, temperature and velocity profiles as well as the mean Sherwood and Nusselt numbers are presented and discussed for different combination of aspect ratios, Rayleigh numbers and buoyancy effects.

Keywords: Buoyancy effects; CVFEM; Heat and mass transfer; Modelling

1. Introduction

There are many transport processes occurring in nature in which flow is driven by density differences caused by temperature,

chemical composition differences and gradients. Despite the intensity of the effort, knowledge in this area is still limited. The demands for additional information and better understanding of this phenomenon have also increased.

*Corresponding author.

*Presented at the Conference on Desalination and the Environment, Santa Margherita, Italy, 22–26 May 2005.
European Desalination Society.*

0011-9164/05/\$– See front matter © 2005 Elsevier B.V. All rights reserved

Natural convection in fluid-filled rectangular enclosures driven solely by a temperature difference has received attention over the past several years because of its numerous engineering applications. These applications span such diverse fields as passive solar heating, solar collectors and the energy efficient design of buildings and rooms to name a few. Extensive reviews for thermal natural convection in enclosures can be found in references [1–3]. However, natural convection flow in rectangular enclosure arising from differences in concentration and in conjunction with temperature effects has received little attention. The mathematical complexities are much more involved than in the purely thermal diffusion problems because of the multiple mass and heat transfer parameters which are correlated in terms of a combined buoyancy effect. The lack of the numerical studies in this area is due to the coupling and non-linearity of the governing equations and the influence of the combined effect on the stability of laminar flows. Furthermore, it is difficult to infer useful information from previous studies regarding mass and heat transfer affecting the distillation rate. In fact, the fluid motion, the mass and thermal structure fields are strongly dependent on the geometrical parameters of the cell and on the mass and thermal conditions. So, the results from one case are not transposable to another case.

Processes involving mass transfer effects have long been recognized as important, principally in chemical processing equipment and in the solar thermal systems that produce potable water from salty water. There are many methods of converting brackish water into potable water using solar energy. The oldest and most widely used process is the capillary film distiller (DIFICAP) which can be integrated in a greenhouse roof by using a glazing cavity [4]. This capillary film distiller presents the advantage of heat recovery: it

is the reuse of the vapour condensation heat to evaporate another quantity of water. This type of distiller has been patented by R. C. Ouahes and P. Le Goff and is made up of identical evaporation-condensation cells [5]. In each cell, a wall on which flows a thin seawater film, is submitted to a solar flux while the opposite wall is maintained at a cooled temperature [6]. In the case of solar distillation systems integrated in a greenhouse roof, the seawater is partially evaporated under the greenhouse effect due to the solar radiation. The condensation water trickles down the external glass and is collected in a tank, which supplies the greenhouse with fresh water for irrigation.

In order to deepen the understanding of the mass and heat transfer mechanisms by natural convection in such processes, a basic study of the problem simulating the situation described above was developed.

The present study is based upon a numerical solution to the complete Navier-Stokes concentration and energy equations for steady state laminar natural convection flow resulting from the combined buoyancy effects of thermal and mass diffusion in a rectangular enclosure with differentially heated side walls. Results are obtained for different combinations of aspect ratio, mass and thermal Rayleigh numbers and the relative importance of chemical and thermal diffusion in causing the density difference.

2. Physical problem and governing equations

Fig. 1 presents a schematic drawing of the considered enclosure which simulates an evaporation-condensation cell of the solar distiller. The study domain is a two dimensional rectangular enclosure of dimension $H \times L$ with different aspect ratios ranging from 1 to 4. The cavity is assumed to be infinite depth along the z -axis and is heated differentially

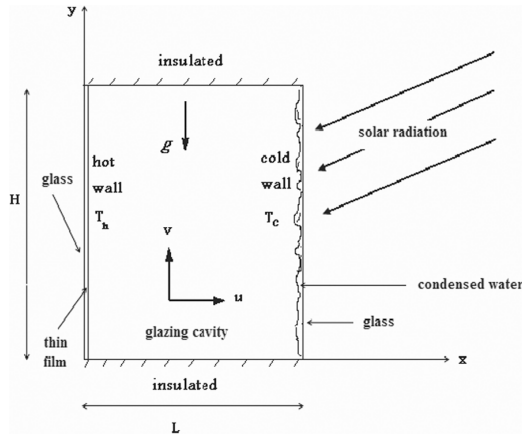


Fig. 1. Geometric configuration the glazing cavity.

along the vertical walls. The left and right walls are held at uniform temperatures, T_h and T_c , respectively, with $T_h > T_c$. The remaining horizontal walls were kept adiabatic in the process. The water on the left hot wall of the cavity is vaporized from the liquid–vapour interface (thin water film). The vapour moves through the air and condenses at the cooled right wall. Conservation equations are written using the stream function–vorticity approach and assuming constant property except for the density in the body force term. The coupled elliptic transport equations for ψ^* , ω^* , C^* and T^* written in Cartesian coordinates, in dimensionless form and for steady 2-dim laminar convection, are as follows:

– Continuity equation:

$$\frac{\partial^2 \psi^*}{\partial x^{*2}} + \frac{\partial^2 \psi^*}{\partial y^{*2}} = -\omega^*$$

– Vorticity equation:

$$U^* \frac{\partial \omega^*}{\partial x^*} + V^* \frac{\partial \omega^*}{\partial y^*} = Ra_T Pr \frac{\partial T^*}{\partial x^*} + Ra_M Pr \frac{\partial C^*}{\partial x^*} + Pr \left[\frac{\partial^2 \omega^*}{\partial x^{*2}} + \frac{\partial^2 \omega^*}{\partial y^{*2}} \right]$$

– Energy equation:

$$U^* \frac{\partial T^*}{\partial x^*} + V^* \frac{\partial T^*}{\partial y^*} = \left[\frac{\partial^2 T^*}{\partial x^{*2}} + \frac{\partial^2 T^*}{\partial y^{*2}} \right]$$

– Mass equation:

$$U^* \frac{\partial C^*}{\partial x^*} + V^* \frac{\partial C^*}{\partial y^*} = \frac{Pr}{Sc} \left[\frac{\partial^2 C^*}{\partial x^{*2}} + \frac{\partial^2 C^*}{\partial y^{*2}} \right]$$

The boundary conditions corresponding to the considered problem are as follows:

- On the hot vertical wall: $T^* = C^* = 1$, $U^* = V^* = \psi^* = 0$
- On the cold vertical wall: $T^* = C^* = 0$, $U^* = V^* = \psi^* = 0$
- On the adiabatic walls: $\partial T^* / \partial y^* = \partial C^* / \partial y^* = U^* = V^* = \psi^* = 0$

We derive the boundary condition for ω^* by expanding the stream function near the wall as a Taylor series and then using the continuity and the no-slip condition: $\omega^* = 2[(\psi_w^* - \psi^*) / \Delta n^{*2}]$.

n^* denotes the normal direction from the wall, ψ_w^* is the stream function value at the wall and ψ^* is the value at a short distance Δn^* into the fluid.

The system of the governing equations contains multiple dimensionless parameters: Ra_T , Ra_M , N , A , Pr and Sc . Buoyancy ratio N represents the relative effect of chemical species diffusion on the thermal diffusion in causing the density difference which drives the flow. It is to be noted that for $N = 0$, there is no mass diffusion effect and the buoyancy force arises solely from the temperature difference. The buoyancy forces from mass and thermal diffusion are combined to assist the flow when $N > 0$, whereas they oppose each other as $N < 0$.

3. Solution procedure

The coupled elliptic transport equation for ψ^* , ω^* , C^* and T^* are solved numerically

using the Control-Volume based Finite-Element Method [7,8]. The most attractive feature of this approach is the physically meaning full basis of its formulation in terms of fluxes and sources and its ability to use an irregular grid which provides more flexibility in fitting irregular domains. The principal advantage of this method is its demonstrated ability to reduce cross-stream diffusion significantly by properly taking into account the local orientation of the flow field. Moreover, the CVFEM provides accurate predictions and physically realistic results with relatively coarse meshes. To overcome instabilities related to the discretization of the velocity components by Linear Interpolation function (LI), we used a Mass-Weighted skew upwind interpolation scheme (MAW) [9]. According to the values of local velocity, we used a hybrid scheme which consists to use the LI scheme, whenever possible, and switch to the MAW scheme when negative contributions to the coefficients in the convection-diffusion discretization equations are encountered.

The discretized equations obtained form a set of simultaneous linear equations. Any suitable solution method can be employed at this stage. In our study, the discretized equations, one for each control-volume, are solved by using the Simultaneous Overrelaxation Method (S.O.R) with Chebyshev acceleration algorithm [10]. The solution was considered converged when the relative error between the new and the old values of and T^* is less than 10^{-4} . We use an unequally spaced grid that provides good results with a minimum number of computational points. In the present study, the number of grid points in the x-direction is fixed at 20 for all cases, while the number of grid points in the y-direction varies from 20 for $A = 1$ to 80 for $A = 4$.

4. Numerical results

The flow, mass and temperature fields are presented for $Pr = 0.7$ and $Sc = 0.6$ which cover water vapour diffusion into air. The thermal Rayleigh numbers Ra_T were varied between 10^0 and 10^5 for two aspect ratios 1 and 4, with two buoyancy ratios 0 and 1. Several computed results for isotherms are shown in Fig. 2. As can be seen, the flow, mass and thermal fields are strongly dependent on thermal Rayleigh number and on the aspect ratio of the enclosure.

The isotherms show steep temperature gradient near the heated wall portion. We note the presence of a thermal plume close to the hot active surface where steep mass and temperature gradients exist. These mass and heat gradients initiate and maintain the natural convection flow within the enclosure. Warm fluid adjacent to the hot surface is convected upward and is replaced by cooled air. In fact, the ascending streams are warmer than the descending ones, providing the driving force in the respective direction of motion.

The similarities between the governing equations for heat and mass transfer suggest that empirical correlation for the mass transfer coefficient and concentration field would

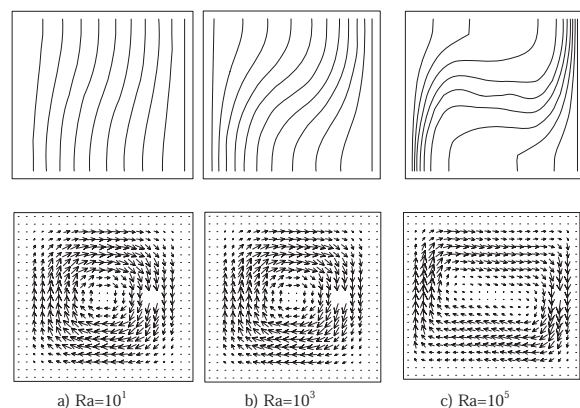


Fig. 2. Isotherms and vector fields for $A = 1$ and $N = 1$.

be similar to those for the heat transfer coefficients and temperature field. So the concentration fields are not presented here because the same change is observed. For low thermal Rayleigh number Ra_T , the isotherms are nearly parallel to the vertical heated wall, indicating that most of the heat transfer is by heat conduction. The effect of convection is seen as the departure of the isotherms from the vertical. As the Rayleigh number increases, the deformation of the isotherms becomes more accentuated and the mechanism of heat transfer is gradually shifted to natural convection.

At $Ra_T = 10^5$, we note also the beginning of the formation of a thermal boundary layer adjacent to the vertical walls. With further increase in thermal Rayleigh number, the boundary layers become thin and more distinguished. The corresponding velocity vector fields shown in Fig. 3, form a nearly centrally located single clockwise rotating vortex. This rotating cell is generated by the temperature gradient across the section. This gradient $\partial T^*/\partial x^*$ is negative everywhere in this case (single rotating cell for $Ra_T \leq 10^5$), giving rise to positive (clockwise rotation) vorticity. We note that this clockwise motion convects cool fluid along the cold wall and down into the lower right-hand quadrant of the enclosure resulting in a negative temperature perturbation. At the same time, warm fluid adjacent to the vertical hot surface is convected upward where it appears as a positive temperature perturbation in the upper portion of the enclosure. As the thermal Rayleigh number increases ($Ra_T \geq 10^4$) the velocity field in the centre of square cavity is distorted into an elliptic shape and the effect of convection is more pronounced in the isotherms. Temperature gradients are now more severe near the vertical walls, but diminish in the centre. This behaviour continues to $Ra = 10^5$ where the velocity field in the centre of the square cavity

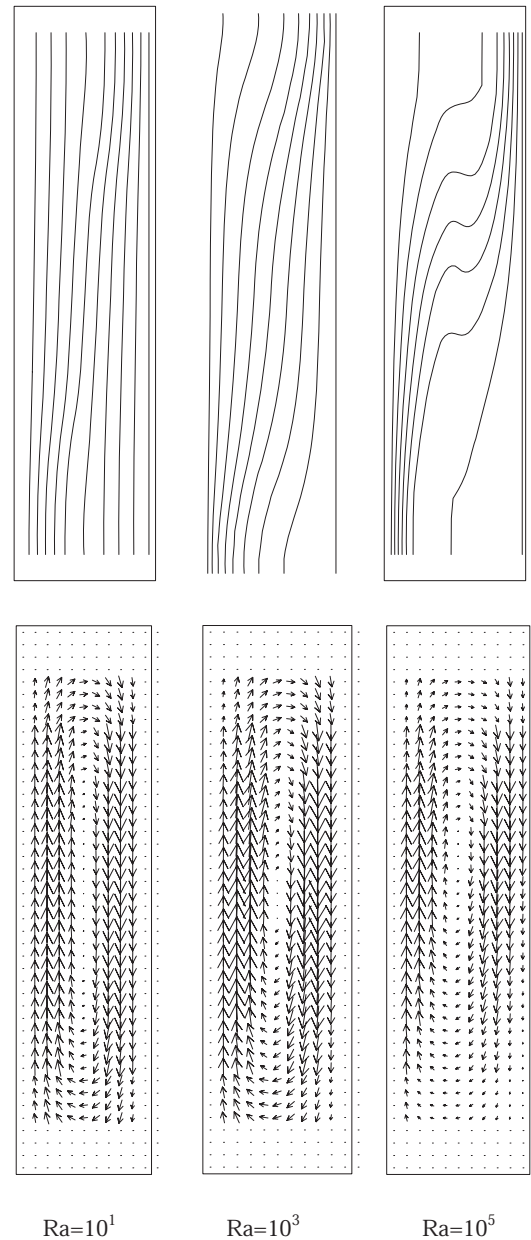


Fig. 3. Isotherms and vector fields for $A = 4$ and $N = 1$.

is further elongated and two small secondary cells appear within the main cell. Heat transfer by convection in the viscous boundary layers alters the temperature distribution to

such an extent that temperature gradients in the centre are close to zero, or change sign, thus promoting negative vorticity. This causes the development of secondary vortices in the core.

As discussed in ref. [2], the secondary vortices in the square cavity do not result from instability of the base flow but are a direct consequence of the convective distortion of the temperature field. As thermal Rayleigh number increases, the development of thermal boundary layers intensifies $\partial T^*/\partial x^*$ in the vicinity of the walls and the convection within each layer leads to the positive $\partial T^*/\partial x^*$ in the centre. A vorticity sink thus separates the regions of concentrated vorticity generation and two vortices are formed. Viscous diffusion appears to prohibit the development of these vortices for $Ra_T < 10^5$. The vortices at $Ra_T = 10^5$ are sufficiently strong to convect the temperature fields to the extent that the isotherms are nearly horizontal in the centre, preventing any vertical motion.

For $A = 4$, the same change of temperature, mass and velocity fields is observed in the enclosure (Fig. 3). However, the variation of thermal Rayleigh number in the considered Rayleigh range ($Ra_T \leq 10^5$) does not affect considerably the flow, mass and temperature fields, persisting on a regime closer to that of conduction. In fact, the structure of velocity and temperature fields suggest that the flow pattern is characterized by a nearly centrally located single clockwise rotating vortices and the deformation of the isotherms becomes less accentuated.

Fig. 4 shows the variation of the vertical velocity component profiles along the horizontal line passing by the geometrical centre of the cavity for two aspect ratios $A = 1$ and $A = 4$ and for two buoyancy numbers $N = 0$ and $N = 1$. It is found for a square cavity that as the thermal Rayleigh number increases, the maximum

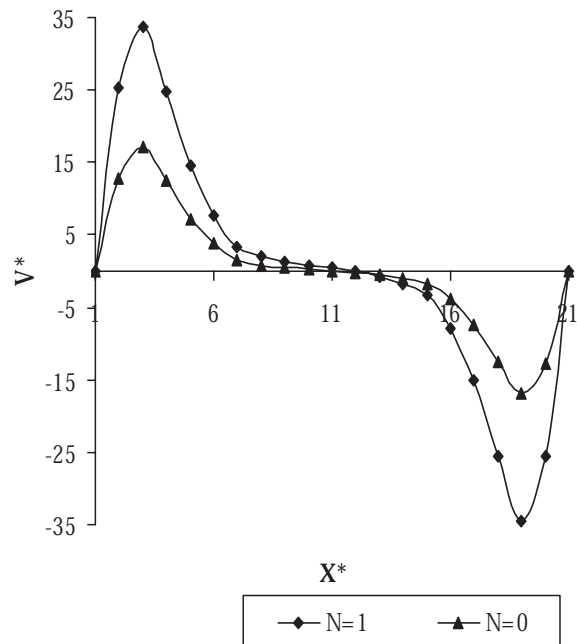


Fig. 4. Vertical velocity component profiles for $Ra = 10^5$.

velocity moves closer to the wall and its amplitude increases. At the same time, the velocity between the two maxima becomes progressively smaller. This indicates that at $Ra_T = 10^5$, the horizontal variation of the vertical velocity is more concentrated at the left and right extremities of the square cavity while along the remaining part of the cavity length, there is no variation. For aspect ratio $A = 4$, the regions of the horizontal variation of the vertical velocity are extended away from the left and right extremities and hence V^* varies along the whole length of the cavity. The buoyancy ratio N represents the ratio of the concentration to thermal buoyancy. It is clear that as compared to the case of $N = 0$ (i.e. the case in which there is no mass diffusion effect and the buoyancy force arises only from the thermal variation), the velocity level increases in the enclosure when the buoyancy force from

species diffusion acts in the same direction of the thermal buoyancy force ($N = 1$).

After convergence is attained, the local Nusselt and Sherwood numbers related respectively to the dimensionless temperature and concentration, and average Nusselt and Sherwood numbers (determined by the Simpson method) are calculated as follows:

$$N_u = \frac{h_t L}{\alpha} = -\frac{1}{Ra_T^{1/2}} \left(\frac{\partial T^*}{\partial x^*} \right); \quad Nu_{av} = \frac{1}{L} \int_0^L N_u dl$$

$$Sh = \frac{h_m L}{D} = -\frac{1}{Ra_M^{1/2}} \left(\frac{\partial T^*}{\partial x^*} \right); \quad Sh_{av} = \frac{1}{L} \int_0^L S_h dl$$

The influence of thermal Rayleigh number on respectively average Nusselt number is shown in Fig. 5. As indicated in previous studies, the heat (mass) transfer is an increasing function of thermal (mass) Rayleigh

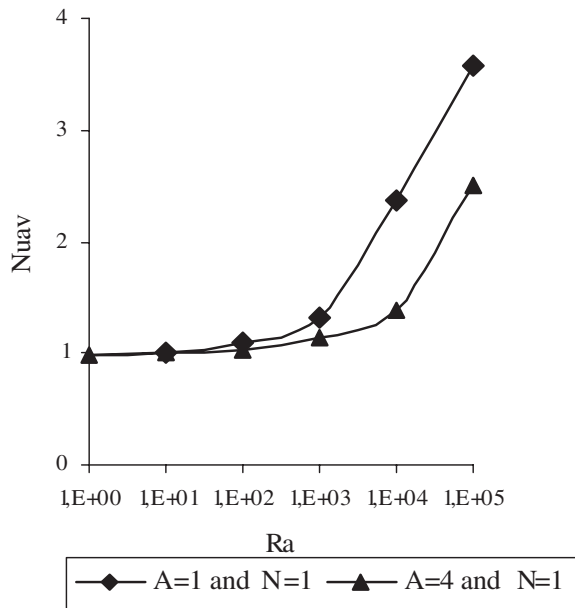


Fig. 5. Variation of average Nusselt number with Rayleigh number.

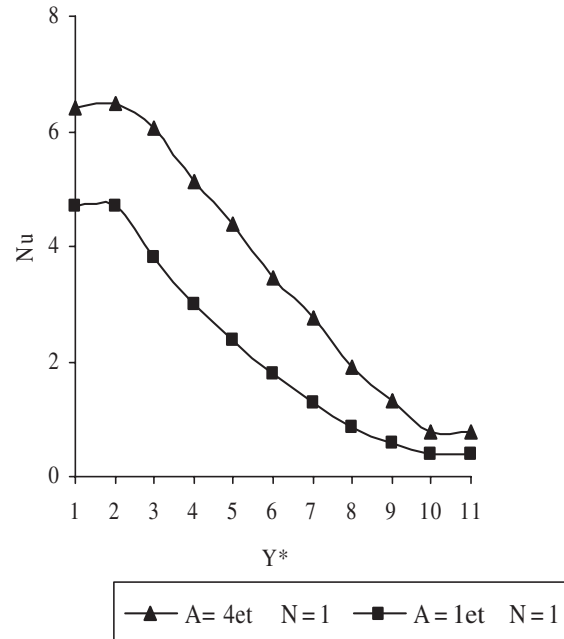


Fig. 6. Local Nusselt for $Ra = 10^5$.

number. The variation of the local Nusselt is presented in Fig. 6. One can notice that the Nusselt number greatly changes with the cavity height indicating a weak maximum value closer to the bottom of the cavity. Also, the curve is characterized by a very weak slope at the vertical extremities. These results are similar to those reported in references [1–3].

5. Conclusion

Numerical solutions to the Navier-stokes, mass and energy equations for laminar natural convection flow resulting from the combined buoyancy effects of thermal and mass diffusion in a cavity with differentially heated side walls have been obtained for large range of Rayleigh numbers and using a control-volume based finite-element method. This numerical approach allowed us to analyse the complex natural convection flow situations arising in the cavity, and appears to be

sufficiently versatile to permit computation of other effects like the inclination of the glazing cavity.

6. Symbols

A	—	Aspect ratio (H/L)
$D_{w;a}$	—	Diffusion coefficient
g	—	Gravitational acceleration, m/s^2
H	—	Height of the enclosure, m
L	—	Length of the enclosure, m
Le	—	Lewis number (Sc/Pr)
N	—	Buoyancy number
Pr	—	Prandtl number (ν/α)
Ra_T	—	Thermal Rayleigh number (based on L) ($\beta_T g (T_h - T_c)L^3/\nu \alpha$)
Ra_M	—	Mass Rayleigh number (based on L) ($\beta_M g (C_h - C_c)L^3/\nu \alpha$)
Sc	—	Shmidt number ($\nu/D_{w;a}$)
T	—	Average temperature, K
T^*	—	Dimensionless temperature $(T - T_c)/(T_h - T_c)$
U^*	—	Dimensionless horizontal velocity $(U L/\alpha)$
V^*	—	Dimensionless vertical velocity $(V L/\alpha)$
x^*	—	Dimensionless x coordinate (x/L)
y^*	—	Dimensionless y coordinate (y/L)

Greek symbols

α	—	Thermal diffusivity, m^2/s
ρ	—	The diffusion coefficient
β_T	—	Coefficient d'expansion thermique du fluid, K^{-1}
β_M	—	Mass expansion coefficient, $m^3 \cdot mol^{-1}$
C	—	Dimensional specie concentration, $mol \cdot m^{-3}$
ν	—	Cinematic viscosity, $m^2 \cdot s^{-1}$
ω	—	Vorticité, s^{-1}
ω^*	—	Dimensionless vorticity $(\omega L^2)/\alpha$
ψ	—	Stream function, m^2/s
ψ^*	—	Dimensionless stream function (ψ/α)

C^*	—	Dimensionless specie concentration $(C - C_c)/(C_h - C_c)$
-------	---	--

Subscripts

av	—	Average
c	—	Cold
h	—	Hot

References

- [1] B. Gilly, P. Bontoux and B. Roux, Influence des conditions thermiques de paroi sur la convection naturelle dans une cavité rectangulaire verticale, différenciellement chauffée, Int. J. Heat Mass Transfer, 24 (1981) 829–841.
- [2] N.C. Markatos and K.A. Pericleous, Laminar and turbulent natural convection in an enclosed cavity, Int. J. Heat Mass Transfer, 27 (1984) 755–772.
- [3] K.A.R. Ismail and V.L. Scaloni, A finite free convection model for the side wall heated cavity, Int. J. Heat Mass Transfer, 43 (2000) 1373–1389.
- [4] M.T. Chaibi, Analysis by simulation of a solar still integrated in a greenhouse roof, Desalination, 128 (2000) 123–138.
- [5] R. Ouahes, P. Le Goff and C. Ouaher, The multi-stage capillary film distiller, CNRS Patent, 2 583 738, 1986, INPI, Paris, France.
- [6] S. Ben Jabrallah, A. Belghith and J.P. Corriou, Study of heat and mass transfer in a rectangular cavity: application to a distillation cell, Int. J. Heat Mass Transfer, 45 (2002) 891–904.
- [7] B.R. Baliga and S.V. Patankar, A control volume finite-element method for two-dimensional fluid flow and heat transfer, Numerical Heat Transfer, 6 (1983) 245–261.
- [8] P. Salagnac, Application d'une méthode d'éléments finis basée sur le concept des volumes de contrôle à la résolution de problèmes de mécanique des fluides et thermique présentant notamment des singularités aux frontières, thèse de doctorat, Université de Poitiers, France, (1995).
- [9] C. Masson and R. Baliga, A control-volume finite element method for dilute gaz-solid particle flows, Computers Fluids 23 (1994) 1073–1096.
- [10] W.T. Vetterling, Numerical Recipes, Cambridge University Press, New York USA 1989.